JOURNAL OF GUIDANCE, CONTROL, AND DYNAMICS
Vol. 18, No. 5, September–October 1995

Fuel-Optimal Stationkeeping via Differential Inclusions

Renjith R. Kumar* and Hans Seywald†
Analytical Mechanics Associates, Inc., Hampton, Virginia 23666

Stationkeeping of one spacecraft in low Earth orbit with respect to another, or with respect to a reference point in space, is a common orbit maintenance and guidance requirement. This paper deals with formulating a infinite time fuel-optimal control problem using the Hill equations (also known as the Clohessy–Wiltshire equations) and solving it via a direct approach using concepts of hodograph space and differential inclusions. The differential inclusion based direct method has been selected due to its excellent convergence robustness. Using this methodology, numerous optimal solutions corresponding to various differential drag profiles and stationkeeping error tolerances were easily obtained from trivial initial guesses. The major contribution of this paper is the interesting observation made regarding the structure of the fuel-optimal solutions as a function of the differential drag profiles and stationkeeping error tolerances. Results from this study can be used for estimating fuel budgets and developing fuel-optimal stationkeeping guidance laws.

Introduction

STATIONKEEPING of two or more satellites is required for missions such as the gravity and magnetic Earth surveyor (GAMES). The GAMES[1] mission consists of one passive aerodynamically stabilized subsatellite P in an initial circular orbit of 325 km. An active satellite A must remain within a distance of 200 km of P with a prescribed tolerance of ± 50 km to perform laser ranging. The relative positions of the two spacecraft are shown in Fig. 1. The altitude decays from 325 to 250 km during the six month life of the mission. The range rate between the two satellites measured by the laser is used to map the Earth's gravitational field. The stationkeeping should ideally be performed using minimal fuel with long quiescent times between stationkeeping thrust firings to accommodate onboard science experiments. Similar stationkeeping requirements are foreseen for the dual Earth observing system (EOS) satellite missions where the two satellites must fly over the same point on the Earth with prescribed time separation and error tolerance.

In this paper, the relative motion of two satellites in near-circular low Earth orbits is addressed. The linearized equations of relative motion, commonly referred to as the Hill equations[2] or the Clohessy–Wiltshire equations,[3] are used to analyze fuel-optimal maneuvers for the active satellite. These linearized equations of relative motion have been previously used successfully for analysis of fuel-optimal rendezvous[4,5] and autonomous rendezvous using fuzzy logic controllers.[6]

The cost index subject to minimization is the fuel consumption by the active satellite for stationkeeping. The error tolerances for stationkeeping become second-order state inequality constraints.[7] A single throttleable jet along the velocity axis is assumed to be the sole control for the active satellite.

The optimal control problem is formulated and the solution is attempted using concepts of differential inclusions.[8,9] This is a direct method[10] where the state variables at prescribed time nodes are the parameters. The feasible state rates are defined by a convex or convexized hodograph space[11] or velocity set.[12] The hodograph space is represented by suitable inequality constraints relating states and state rates. The major advantage of this scheme over conventional collocation methods[13] is that the control variables are completely eliminated as parameters. This prevents the need for guessing the rapidly changing control time history, eliminates the nonuniqueness of control representation, and reduces the number of parameters involved in the optimization problem. Moreover, in the presence of singular arcs, as for the benchmark Goddard problem,[7] the differential inclusion methodology has shown improved convergence robustness.[14]

The major perturbation on the relative motion of the two satellites is assumed to be due to differential drag. The differential drag consists of a bias component and periodic terms at orbit frequencies, such as due to diurnal bulge effect,[15] and higher harmonics, such as due to solar array articulation. The major influence on the fuel consumption is due to the bias component and the periodic term at orbit frequency. It is shown in this paper that perturbations of higher frequencies can be ignored for fuel calculations for reasonable error tolerances in stationkeeping. The effects due to differential solar radiation pressure and differential third-body effects are assumed to be small in comparison to differential drag and hence ignored in this study. The major contribution due to J_2 is to precess the orbit,[15] which is similar for both spacecraft, independent of mass. The predominant frequency in the differential J_2 acceleration is at twice orbit rate, corresponding to the Earth's longitudinal bulge and is ignored for the same reason as for the higher harmonics of differential drag.

Problem Formulation

What is the minimum fuel requirement for stationkeeping of one satellite with respect to another in a low Earth circular orbit? What are the associated optimal control strategies? The stationkeeping problem may be defined as the translational maneuvers required to ensure that either 1) the two satellites are spacially separated by a prescribed distance $\bar{\Lambda}$ with a tolerance of $\pm\bar{\lambda}$ or 2) the two satellites would fly over the same point on the Earth separated by a prescribed time T with a tolerance of $\pm\varepsilon$.

For circular orbits and large tolerances, it is tacitly assumed that the spacial separation problem and the time separation problem just defined have similar fuel requirements. Hence, only the spacial separation problem is examined in this study. The schematic of the constraint box about a target point X is shown in Fig. 1. The active satellite must at all times remain inside the constraint box. The target point is a function of position of P and $\bar{\Lambda}$, and the box size depends on the tolerance $\pm\bar{\lambda}$. The motion of the target point is completely determined by the motion of the passive satellite.

Mathematical Modeling

The Hill equations are used to describe the relative dynamics between the two satellites. The assumptions used to derive the Hill equations are 1) circular orbit (the eccentricity of the passive vehicle orbit or the target orbit is zero), 2) the geopotential is inversely proportional to the distance to the center of the Earth (in other words, J_2 and other higher geopotential terms are ignored), and 3) linearized equations in the vicinity of the target point.

Received Aug. 25, 1994; revision received March 13, 1995; accepted for publication May 28, 1995.

*Senior Engineer. Member AIAA.
†Supervising Engineer. Member AIAA.

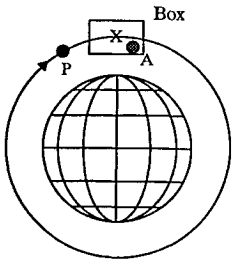

Fig. 1 Relative position of vehicles and constraint box.

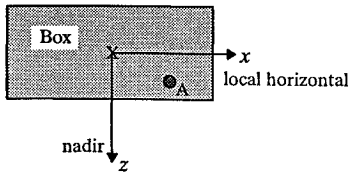

Fig. 2 Coordinate definition.

The out-of-plane dynamics are completely uncoupled from the in-plane dynamics and hence can be treated independently. Since the effect of differential drag is mostly in-plane, the out-of-plane dynamics are ignored. The in-plane dynamics are described by the following first-order differential equations:

$$\dot{x} = V_x \tag{1}$$

$$\dot{z} = V_z \tag{2}$$

$$\dot{V}_x = 2nV_z + d_x + u_x \tag{3}$$

$$\dot{V}_z = 3n^2 z - 2nV_x + d_z \tag{4}$$

$$\dot{m}_p = \frac{m_a |u_x|}{c} \tag{5}$$

The differentiation $(\cdot)$ is with respect to real time t. Figure 2 depicts the coordinate system with the origin at the target point. Here, x and z denote the in-plane position of the active satellite A with respect to the target point. The relative velocity of A with respect to the target point X is given by V_x and V_z. In the preceding equations, the constant n denotes the orbit rate. All numerics presented in this paper assume an altitude of 250 km. The term d_x denotes the differential drag acceleration along local horizontal, and d_z is the differential drag acceleration along nadir. The propellant consumed is denoted by m_p and the mass of the active satellite m_a is assumed to be constant (325 kg), since it is large compared with the propellant used. The constant exhaust velocity of the control jet is given by $c = I_{sp}g$, where I_{sp} is the specific impulse of the propellant, and g is the acceleration due to gravity at sea level. An I_{sp} of 230 s, corresponding to hydrazine, is assumed in this study. The control acceleration u_x has a lower and upper bound given by the following relation, where $u_{x\max}$ is 0.05538 m/s^2 corresponding to a maximum thrust of 18 N:

$$-u_{x\max} \le u_x \le u_{x\max} \tag{6}$$

For satellites in low Earth orbit most of the disturbing accelerations arise due to differential drag. The major contribution of this is along the x axis. The differential drag accelerations depend on the ballistic coefficients of the two satellites and the spacial separation. The bulge causes the atmospheric densities to be different for the two spacially separated satellites even at identical altitudes. The differential drag acceleration along the velocity vector is given by

$$d_x = \frac{q_A}{B_A} - \frac{q_P}{B_P} \tag{7}$$

where q denotes the dynamic pressure, and B the ballistic coefficients. The subscripts A and P denote the active and passive satellites, respectively. Assuming similar orbital velocities V for both the satellites, Eq. (7) becomes

$$d_x = 0.5V^2\left(\frac{\varrho_A}{B_A} - \frac{\varrho_P}{B_P}\right) \tag{8}$$

The diurnal bulge effect causes the densities ϱ_A and ϱ_P to have a once-per-orbit frequency n in addition to a bias. It can be easily shown that Eq. (8) reduces to

$$d_x = d_{xb} + d_{xa}\sin(nt + \phi) \tag{9a}$$

where d_{xb} corresponds to the bias differential drag and d_{xa} corresponds to the amplitude of the sinusoidal differential drag harmonic at frequency n. The phase angle ϕ is not critical since the station-keeping control problem is addressed over many multiples of orbits. The differential drag acceleration along nadir is assumed to be zero, i.e.,

$$d_z = 0 \tag{9b}$$

The bias differential disturbing acceleration and the acceleration at once-per-orbit frequency impact fuel consumption more than the differential perturbations at higher harmonics. The reason is as follows.

The differential equations (1–4) with zero control acceleration and differential perturbation accelerations of the form

$$d_x = \alpha + \beta\sin(nt + \phi_1) + \gamma\sin(2nt + \phi_2) + \text{higher harmonics} \tag{10}$$

have a closed-form solution

$$z = a + b\sin(nt) + c\cos(nt) - \frac{2\alpha t}{n} + \frac{\beta t}{n}\sin(nt + \phi_1) - \frac{\gamma}{3n^2}\cos(2nt + \phi_2) + \text{higher harmonics} \tag{11}$$

where a, b, and c correspond to constants defined by boundary conditions. The fourth constant appears in the similar closed-form solution of x. The important feature to be noted in the closed-form solution is the fact that the bias and once-per-orbit frequency perturbations cause a secular growth of z, whereas higher order harmonic perturbations keep the solution periodic. If the constraint box is big enough, fuel consumption is required only to accommodate the secular terms. Moreover, the bias and once-per-orbit frequency perturbations are in general predominant compared with other disturbances.

Optimal Control Problem

The statement of the fuel-optimal control problem is as follows:

$$\min_{\{u_x\}} J = \frac{m_p(t_f)}{t_f}; \qquad t_f \to \infty \tag{12}$$

subject to the differential constraints imposed by Eqs. (1–5), the control constraint defined by Eq. (6), and the following state constraints and boundary conditions given by Eqs. (13) and (14), respectively. Here t_f denotes the final time.

The following state constraints are required to ensure that the active satellite is always within the constraint box:

$$\begin{aligned} x_{\min} \le x \le x_{\max} \\ z_{\min} \le z \le z_{\max} \end{aligned} \tag{13}$$

Here, $x_{\min}, x_{\max}, z_{\min}$, and $z_{\max}$ are constants used to define the spacial box constraint.

The following boundary conditions are used for the state variables:

$$\begin{aligned} x(t_0) &= x(t_f) \\ z(t_0) &= z(t_f) \\ V_x(t_0) &= V_x(t_f) \\ V_z(t_0) &= V_z(t_f) \\ m_p(t_0) &= 0 \end{aligned} \tag{14}$$

where t_0 denotes initial time.

Note that the cost index assumes an infinite time problem. In practice, one would systematically increase the final time in multiples M

of orbit periods until the optimal cost J shows convergence for the periodic boundary conditions in the relative position and velocity states. It is clear that the restriction of periodicity does not change the cost as M tends to infinity. Therefore, if the preceding convergence occurs, then that minimum value of M could be utilized for defining the final time in the optimization procedure. Note that the periodicity assumption prevents any final maneuvers (for a fixed time simulation) which would artificially reduce fuel consumption but yield large terminal position (on the constraint box boundaries) and large velocity states.

Numerical Solutions via Differential Inclusions

The optimal control problem described earlier is solved by a direct approach using concepts of hodograph space and differential inclusions algorithm.[9]

The time axis is divided by equally spaced nodes. The five states at each of the nodes are treated as the unknown parameters. The cost function to be minimized is the state m_p at the final node. The differential equations (1–5), the control constraint given by Eq. (6), the state constraints given by Eq. (13), and the boundary conditions given by Eq. (14) need to be enforced. The state constraints turn out to be simple parameter bounds for the position states and are enforced at each node. The periodicity constraint [Eq. (14)] is implemented by equating the position and velocity state vector at the first node to the position and velocity state vector at the last node. Enforcement of the differential constraints and the control constraint are described as follows.

Define the following functions:

$$f_1 = \dot{x} - V_x \tag{15}$$

$$f_2 = \dot{z} - V_z \tag{16}$$

$$f_3 = \dot{V}_x - 2nV_z - d_x \tag{17}$$

$$f_4 = \dot{V}_z - 3n^2 z + 2nV_x - d_z \tag{18}$$

$$f_5 = \dot{m}_p c / m_a \tag{19}$$

At the midpoint of any two neighboring nodes, approximate the states by their average values and evaluate the state rates by central differencing. Thus the functions $f_1 \cdots f_5$ given by Eqs. (15–19) are defined at every nodal midpoint.

The following equations are then used to enforce the differential constraints and the control constraint at every nodal midpoint:

$$f_1 = 0 \tag{20}$$

$$f_2 = 0 \tag{21}$$

$$f_4 = 0 \tag{22}$$

$$f_5 \le u_{x\max} \tag{23}$$

$$f_5 - f_3 \ge 0 \tag{24}$$

$$f_5 + f_3 \ge 0 \tag{25}$$

From the states guessed at each node, the state rates are evaluated and enforced to lie within the hodograph space as schematically shown in Fig. 3. In general, the hodograph space is a function of time and states. For this specific problem, the hodograph space is independent of time and states; i.e., the shape does not change with respect to time and states. Equations (20–25) completely characterize the evolution of the states. Note that the control is eliminated in this formulation. Strictly speaking, the union of line segments OA and OB, as shown in Fig. 4, is the hodograph space. However, this is nonconvex and needs to be convexized for practical use by any generic nonlinear programming solver. The convexization is performed via Eqs. (23–25) corresponding to the boundary lines l_3, l_2, and l_1, respectively. The convexized hodograph space or the feasible state-rate space is shown by the shaded area in Fig. 4. Note

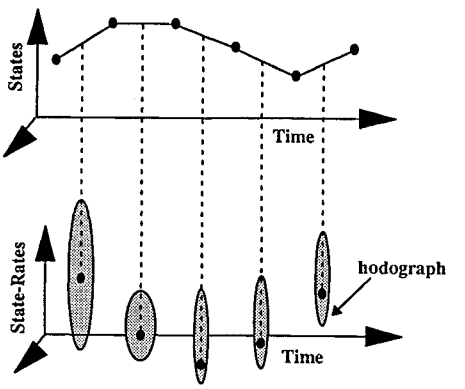

Fig. 3 Schematic of the differential inclusion algorithm.

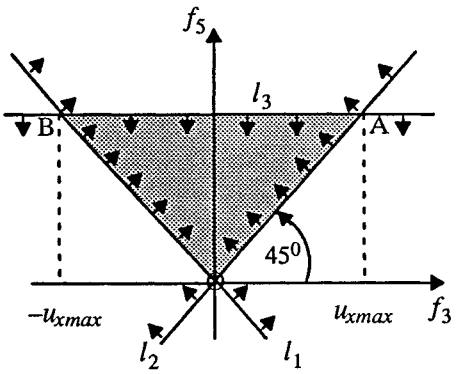

Fig. 4 Hodograph space.

the increase in the allowable hodograph space from the original nonconvex space. However, since fuel is minimized, the nonlinear optimization would automatically result in state rates corresponding to the original nonconvex hodograph.

The resulting parameter optimization problem reduces to minimizing m_p at the final node. The parameters are the states at the nodes, and the constraints include the hodograph, boundary, and state constraints. This problem is solved using a nonlinear programming solver.[16]

Numerical Results

Since infinite time problems cannot be addressed directly by this method, the parameter optimization was performed with final time fixed. It was observed that the cost function given in Eq. (12) was independent of the final time, as long as the final time was an integer multiple of the orbit period, assuming the same nodal discretization per orbit. Thus, optimizations (with 151 equally spaced nodes) over only one orbit needed to be performed. The larger the number of nodes, the smaller the error involved in linearization assumptions. However, due to limited computer memory, no finer discretization was possible. The number of parameters was 755 (151 nodes × 5 states) and the number of constraints not including the parameter bounds was 904 (150 midpoint of nodes × 6 differential constraints +4 periodicity constraints). Optimizations were performed for different drag profiles and constraint box sizes, assuming the box to be a square of length l meters.

Figure 5 shows the variation of optimal fuel used for different values of d_{xb} and box sizes. The amplitude of cyclic drag acceleration was d_{xa} kept constant at 0.00083 m/s^2. This large value of d_{xa}, on the order of milli-g, was used to prevent masking of the fuel calculations due to artificial buildup of numerical errors induced by the discretization and the central differencing. This problem may be overcome by increasing the number of nodes or increasing the order of implicit integration. A later section deals with an exact integration methodology that overcomes this problem. The graphs with legends 1–9 in Fig. 5 are for d_{xb} corresponding to 0.83e-3, 0.7e-3, 0.6e-3, 0.5e-3, 0.415e-3, 0.3e-3, 0.2e-3, 0.1e-3 m/s^2 and zero bias, respectively.

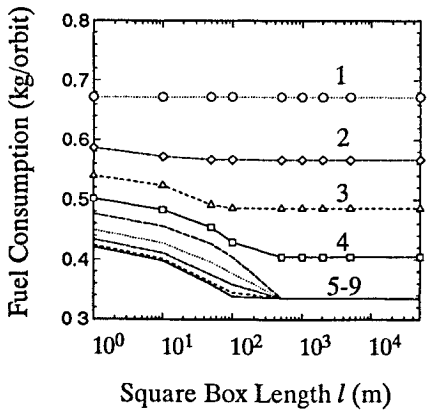

Fig. 5 Variation of fuel consumption.

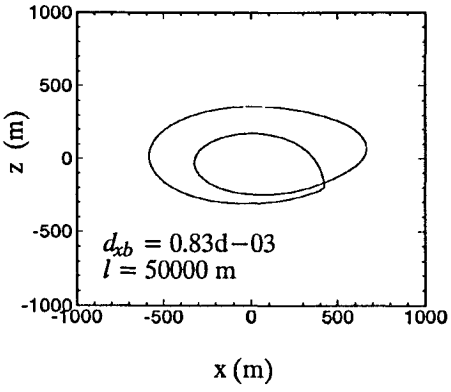

Fig. 6 x-z trajectory.

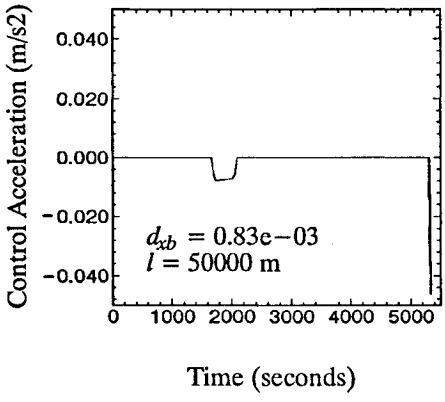

Fig. 7 Control acceleration time history.

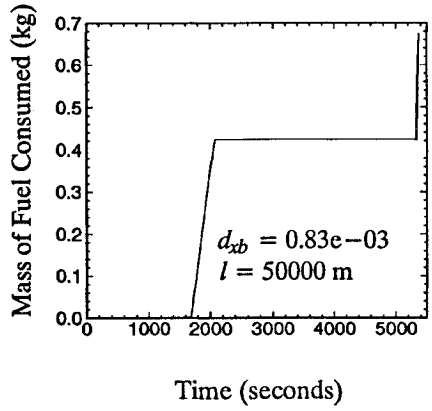

Fig. 8 Mass of fuel consumed.

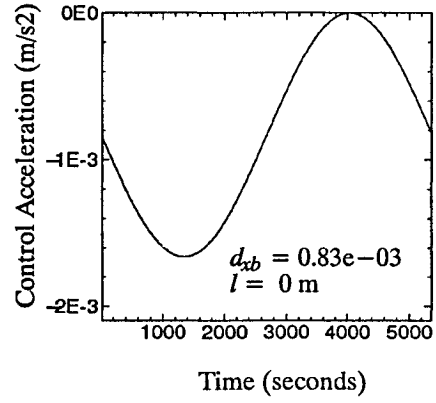

Fig. 9 Control acceleration time history.

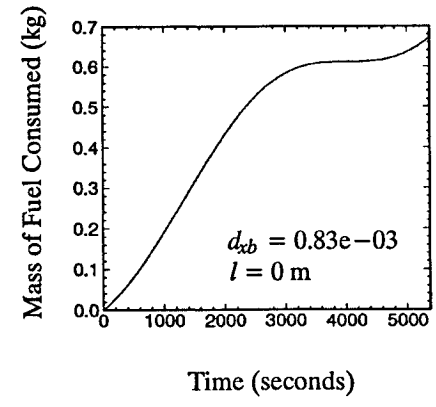

Fig. 10 Mass of fuel consumed.

Case 1

If $d_{xb} \geq d_{xa}$, as for graph 1 of Fig. 5, where $d_{xb} = d_{xa}$, it can be observed that the fuel consumed is independent of the box size. For a large box of length 50 km, one of the optimal x-z closed trajectories is shown in Fig. 6. The optimal control acceleration and fuel consumption are shown in Figs. 7 and 8, respectively. For the limiting case, where the box is of zero length, the control acceleration must be equal to the negative of the drag acceleration as shown in Fig. 9. The total fuel consumed per orbit for this case, as shown in Fig. 10, is proportional to d_{xb} and is the same as that shown in Fig. 8. It is to be noted here that for the zero size box the fuel consumption can be calculated via simple algebraic equations since the control acceleration must equal the negative of the differential drag acceleration. The fuel numbers calculated from this method and the optimal solution of the 50-km constraint box match to the seventh significant digit. Similar observations were made for the stationkeeping problem when $d_{xb} > d_{xa}$. Thus, one can conclude that if $d_{xb} \geq d_{xa}$, there exist nonunique fuel-optimal strategies, all of which yield the same cost, and the cost is dependent only on the magnitude of d_{xb}. An immediate guidance strategy that becomes obvious for such cases is a simple drag makeup strategy using some learning algorithms such as neural networks, which would estimate the differential drag. On the other hand, one could utilize the nonuniqueness of the fuel-optimal strategy and enforce the total fuel consumption as a constraint and optimize other criteria, such as maximizing the quiescent time between thrusts.

Case 2

If $d_{xa} > d_{xb} \geq d_{xa}/2$, as shown by graphs 2–4 of Fig. 5, for large box sizes ($l > 500$ m, which are typical mission scenarios), the fuel consumption is independent of the box size. However, for small box sizes, the fuel consumption increases as the box constraint is made tighter. The left extreme of the graphs 2–4 show fuel consumptions corresponding to drag makeup strategies, and the right extremes of the graphs depict fuel consumptions corresponding to a drag makeup strategy as if d_{xa} were zero.

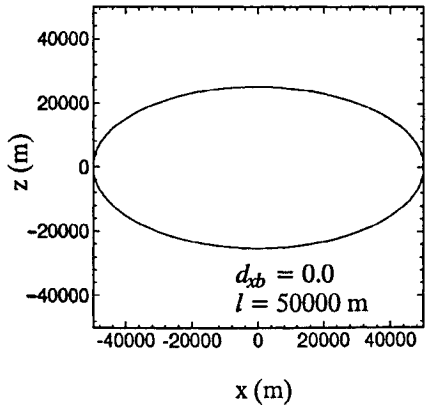

Fig. 11 x-z trajectory.

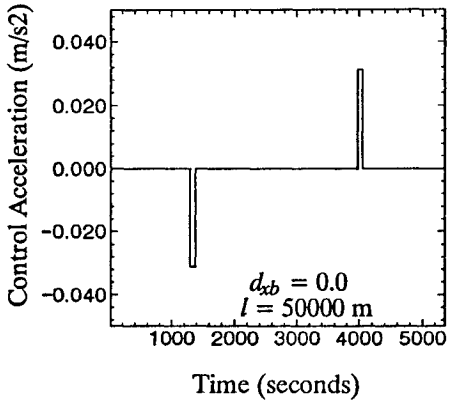

Fig. 12 Control acceleration time history.

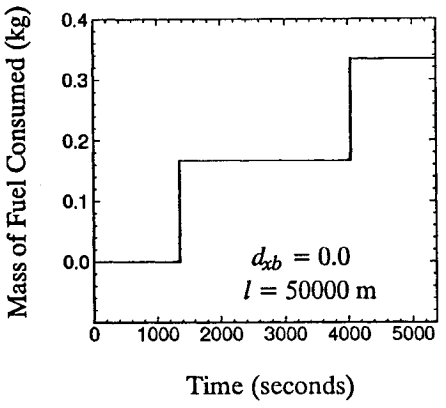

Fig. 13 Mass of fuel consumed.

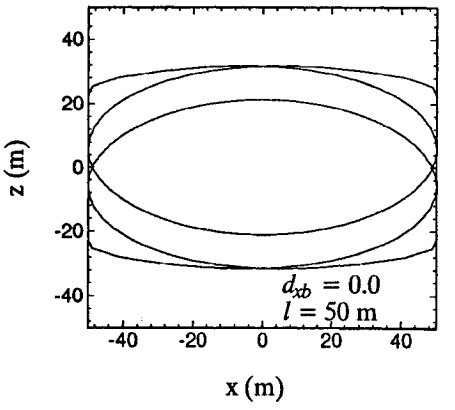

Fig. 14 x-z trajectory.

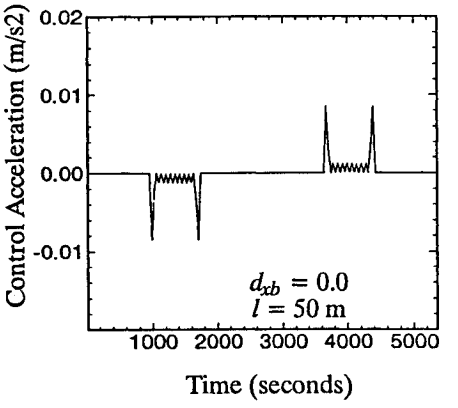

Fig. 15 Control acceleration time history.

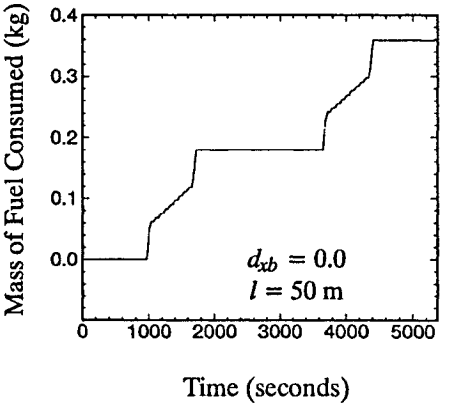

Fig. 16 Mass of fuel consumed.

Case 3

If $d_{xa}/2 > d_{xb} \geq 0$, as shown by graphs 5–9 of Fig. 5, for large box sizes, the fuel consumption is nearly independent of the box size. However, for small box sizes, the fuel consumption increases as the box constraint is made tighter. The left extreme of the graphs 5–9 show fuel consumptions corresponding to drag makeup strategies, and the right extremes of the graphs depict fuel consumptions corresponding to a drag makeup strategy as if only a differential bias drag $d_{xb} = d_{xa}/2$ existed.

Figure 11 shows a football-shaped trajectory for a box size of length 50 km and zero bias. The peak z value is approximately half the peak x motion. The control history in Fig. 12 shows small impulses at either ends of the football trajectory. These types of impulses are ideally suited for off-the-shelf nonthrottleable jets. The fuel consumption is given by Fig. 13.

Similar solutions are shown in Figs. 14–16 for the case where the box length is reduced to 50 m. Active state constraints and touch points[17] can be seen along the x-z trajectory, and the control time history shows chattering behavior along the active state constraint. This chattering is a pseudoeffect of the discretization and can be replaced by an average control and hence an average state rate. The total fuel consumed is more than that shown in Fig. 13. Thus, the fuel budget depends on the error tolerance.

Most of the optimal solutions were obtained from initial guesses where the states were set to zero at all nodes. The utility of a differential inclusion type direct approach is evident when the optimal control time history is complex and hence not intuitive.

Exact Differential Constraints

As stated earlier, the derivatives of the states at the midpoint of the nodes are calculated assuming a simple central differencing approximation. However, as the magnitude of the differential drag used for numerical simulation decreases, the relative error on the fuel calculations introduced by the central differencing approximation increases considerably. This problem could be circumvented by exact integration of the linear differential equations across the nodes, while assuming piecewise constant controls.

Equations (1–5) can be vectorially represented by

$$\dot{y} = [A]y + [B]u + v \tag{26}$$

where the vectors y, u, and v are defined by

$$y \doteq [x \quad z \quad V_x \quad V_z \quad m_p]^T \tag{27}$$

$$u = \begin{bmatrix} u_{1_x} & u_{2_x} \end{bmatrix}^T \tag{28}$$

$$v = [0 \quad 0 \quad d_x \quad d_z \; 0]^T \tag{29}$$

The scalar control u_x in Eq. (3) is broken up into two parts, i.e., $u_x = u_{1_x} - u_{2_x}$ to eliminate the absolute value function in Eq. (5).[18] The control constraint in Eq. (6) takes the following form:

$$0 \leq u_{1_x} \leq u_{x\max} \tag{30}$$

$$0 \leq u_{2_x} \leq u_{x\max} \tag{31}$$

The system matrix A and the control input matrix B are constant matrices given by

The relationship of the states across a node (or equivalently a time interval Δt), assuming piecewise constant control, is given by

$$y(t + \Delta t) = Ey(t) + QBu(t) + P \tag{32}$$

where the matrices E, Q, and P are defined by

$$E = e^{A(\Delta t)} \tag{33}$$

$$A = \begin{bmatrix} 0 & 0 & 1 & 0 & 0 \\ 0 & 0 & 0 & 1 & 0 \\ 0 & 0 & 0 & 2n & 0 \\ 0 & 3n^2 & -2n & 0 & 0 \\ 0 & 0 & 0 & 0 & 0 \end{bmatrix}, \qquad B = \begin{bmatrix} 0 & 0 \\ 0 & 0 \\ 1 & -1 \\ 0 & 0 \\ \frac{m_a}{c} & \frac{m_a}{c} \end{bmatrix}$$

$$Q = \int_{\tau=t}^{\tau=t+\Delta t} e^{A(t+\Delta t-\tau)}\, d\tau \tag{34}$$

$$P = \int_{\tau=t}^{r=t+\Delta t} e^{A(t+\Delta t-\tau)}\, v(\tau)\, d\tau \tag{35}$$

The control elimination and the exact hodograph constraint representation to pose the problem in the differential inclusion format is performed as follows. Define the vector S:

$$S = Bu = Q^{-1}[y(t + \Delta t) - Ey(t) - P] \tag{36}$$

Constant matrices E and Q are evaluated independent of the differential drag. The time-varying matrix P can be evaluated assuming the functional relationships in Eqs. (9) and (29). The symbolic manipulation software MATHEMATICA was used to obtain these matrices.

Define the submatrix B_s that contains the nonzero rows and columns of control input matrix B:

$$B_s = \begin{bmatrix} 1 & -1 \\ \frac{m_a}{c} & \frac{m_a}{c} \end{bmatrix}$$

Define the vector H as

$$H = B_s^{-1} \begin{bmatrix} S(3) \\ S(5) \end{bmatrix}$$

It can be easily verified that the exact differential constraints are

$$S(1) = 0 \tag{37}$$

$$S(2) = 0 \tag{38}$$

$$S(4) = 0 \tag{39}$$

$$0 \leq H(1) \leq u_{x\max} \tag{40}$$

$$0 \leq H(2) \leq u_{x\max} \tag{41}$$

This exact formulation eliminates the error introduced by central differencing approximations. It should be noted that the piecewise constant control approximation is still assumed. This methodology corroborated the results presented in the previous sections for high differential drag in the order of milli-gs. Moreover, for differential drag in the order of micro-gs, the exact method solves the optimal control problem while eliminating any discretization and linearization errors that would otherwise mask the fuel calculations. No increase in the number of nodes is required.

Conclusions

The fuel-optimal stationkeeping control problem was posed and solved via a direct approach utilizing concepts of differential inclusion and hodograph space. Most of the optimal solutions were obtained from zero states guessed at all nodes, indicating the convergence robustness of this approach. Moreover, the utility of this approach is evident when the optimal solutions have complex switching structure and the optimal control time history is not intuitive.

It has been shown that the fuel consumption for stationkeeping maneuvers is independent of stationkeeping error tolerance for the family of differential drag profiles where the differential bias drag is greater than or equal to the once-per-orbit sinusoidal differential drag amplitude. Thus 1) fuel budgeting is easily performed using ideas of simple drag makeup, and 2) a simple learning controller can be used for real-time drag makeup guidance, or 3) the nonuniqueness of the fuel-optimal strategy can be utilized to optimize another criterion, such as maximizing the quiescent time between control thrusts.

For other classes of dragprofiles, the fuel consumption can be bound between an upper bound corresponding to drag makeup and a lower bound with interesting characterizations. These bounds are independent of the tolerance (constraint box size). The preceding conclusion 3 can be made for reasonable size constraint boxes that arise in typical mission scenarios. The minimum constraint box size above which the fuel consumption is independent of the tolerance might be of critical importance to mission design.

Acknowledgment

This work was completed under Contract NAS1-18935 with Space Systems and Concepts Division at NASA Langley Research Center.

References

[1]Anon., "Gravity and Magnetic Earth Surveyor Phase—A Study Report," NASA Goddard Space Flight Center and Center National D'Etudes Spatiales, Toulouse, Oct. 1993.

[2]Kaplan, M. H., *Modern Spacecraft Dynamics and Control*, Wiley, New York, pp. 109–111.

[3]Clohessy, W. H., and Wiltshire, R. S., "Terminal Guidance System for Satellite Rendezvous," *Journal of Aerospace Sciences*, Sept. 1960, pp. 653–658, 674.

[4]Carter, T. E., "Fuel-Optimal Maneuvers of a Spacecraft Relative to a Point in Circular Orbit," *Journal of Guidance, Control, and Dynamics*, Vol. 7, No. 6, pp. 710–716.

[5]Lembeck, C. A., and Prussing, J. E., "Optimal Impulsive Intercept with Low-Thrust Rendezvous Return," *Journal of Guidance, Control, and Dynamics*, Vol. 16, No. 3, pp. 426–433.

[6]Freeman, L. M., KrishnaKumar, K., Karr, C. L., and Meredith, D. L., "Tuning Fuzzy Logic Controllers Using Genetic Algorithms—Aerospace Applications," *Proceedings of the AAAIC'90 Conference* (Dayton, OH), AIAA, Washington, DC, 1990, pp. 351–358.

[7]Bryson, A. E., and Ho, Y. C., *Applied Optimal Control*, Hemisphere, New York.

[8]Aubin, J. P., *Differential Inclusions*, Springer–Verlag, 1984.

[9]Seywald, H., "Trajectory Optimization Based on Differential Inclusions," *Journal of Guidance, Control, and Dynamics*, Vol. 17, No. 3, 1994, pp. 480–487.

[10]Ewing, G. M., *Calculus of Variations*, Dover, New York, 1965.

[11]Cliff, E. M., Seywald, H., and Bless, R. R., "Hodograph Analysis in Aircraft Trajectory Optimization," AIAA Paper 93-3742, Aug. 1993.

[12]Lee, E. B., and Markus, L., "Foundations of Optimal Control Theory," Krieger, Malabar, FL, 1986.

[13]Hargraves, C. R., and Paris, S. W., "Direct Trajectory Optimization Using Nonlinear Programming and Collocation," *Journal of Guidance, Control, and Dynamics*, Vol. 10, No. 4, 1987, pp. 338–342.

[14]Seywald, H., and Kumar, R. R., "NASA SBIR 93-1 Phase-I Final Report," NASA Langley Research Center, Contract NAS1-20131, July 1993.

[15]Wertz, J. R., *Spacecraft Attitude Determination and Control*, D. Reidel Publishing Co., The Netherlands, 1980, pp. 66, 67.

[16]Gill, P. E., Murray, W., Saunders, M. A., and Wright, M. H., "User's Guide for NPSOL: A Fortran Package for Nonlinear Programming," Stanford Univ., TR SOL86-2, Dept. of Operations Research, Stanford, CA, Jan. 1986.

[17]Seywald, H., and Cliff, E. M., "On the Existence of Touch Points for the First-Order State Inequality Constraints," AIAA Paper 93-3743, Aug. 1993.

[18]Seywald, H., Kumar, R. R., Deshpande, S. M., and Heck, M. L., "Minimum Fuel Spacecraft Reorientation," *Journal of Guidance, Control, and Dynamics*, Vol. 17, No. 1, 1994, pp. 21–29.